International Journal of Applied Engineering Research
ISSN 0973-4562 Volume 10, Number 1 (2015) pp. 1-15

http://www.ripublication.com

Differential-Capacitance Instrument For Measurements of Inertial and Gravitational Forces and Torques: Parametric Design (Part 2)

Igor Gilavdary[1], Samir Mekid[2]
[1]*National Technical University of Belarus, Nezavisimosti av.65, Minsk, 220013 Belarus*
[2]*King Fahd University of Petroleum & Minerals, Mechanical Engineering Department, Dhahran, 31261, Saudi Arabia*

Abstract

The theoretical dynamics modeling and design of an electrostatic sensor measuring noncontact harmonic forces and torques, both inertial and gravitation are described. The sensor combines both the electrostatic sensor and electrostatic actuator. The linear differential and algebraic equations were derived in part 1 and the sensor's behaviors at harmonic, transient and resonance processes are investigated. The external and internal types of energy dissipation and their influences on dynamic behaviors as well as the sensor's thermal noise are investigated. The numerical calculations of the sensor's parameters as a resonant gravity gradiometer gauge are described.

Keywords: differential capacitive sensor, capacitive actuator, noncontact forces and torques measurements, resonant gauge, linier accelerometer, angular accelerometer, gravity gradiometer.

Introduction

A simple and sensitive resonant electrostatic differential capacitive force and torque sensor (Fig.1) where a resonant electrical circuit is absent was proposed in Part 1 [1]. The physical and the nonlinear mathematical models of the sensor were derived. The sensor's output signals are currents flowing through two capacitors. The static and dynamic analyses of the sensor's equilibrium were fulfilled. It was shown that electrical asymmetry in differential capacitors imposes severe restrictions on the sensor fabrication.

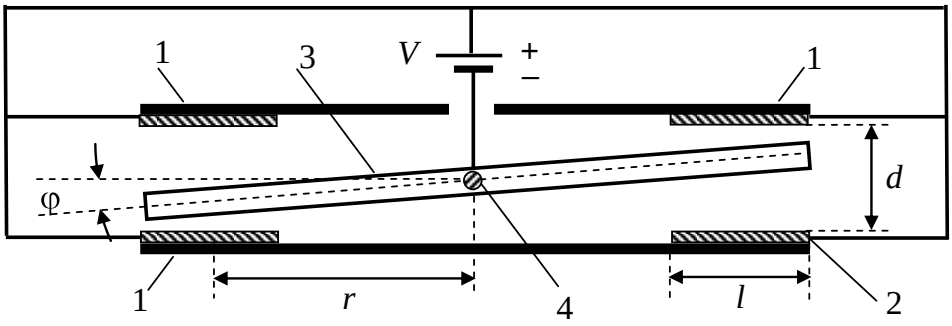

1 – Fixed non-conductive plate, 2 – conductive substrate, 3 –conductive plate, 4 – elastic torsion hanger.

Figure 1: The sensor's diagram

Moreover, it has been shown that one or two additional voltage sources are able to compensate for this asymmetry. In this second part, the equation's order is prolonged compared to those in Part 1 and equations numbers are supplied with '1.' when cited from part 1, e.g. Eq.(1.33).

The sensor with a compensation of an asymmetry is show in figure 1. Here (see also Eqs. (1.3)) $C_1 = \frac{C_{01}}{1+\varphi/\varphi_m}$, $C_2 = \frac{C_{02}}{1-\varphi/\varphi_m}$, where φ – a rotation angle of a moveable sensitive plate (SP) in the sensor; φ_m – a maximal of φ is limited sensor's geometry. In common case $C_{01} \neq C_{02}$. The sensor's electrical asymmetry is described by a parameter γ like it is in an equation $C_{02} = \gamma_1 C_{01}$, where $\gamma_1 = 1+\gamma$. In the Part 1 (Eq. (1.27)) it was shown that the equality $V_2 = \frac{\gamma}{\gamma_1} V + \frac{V_1}{\gamma_1}$, is needed to compensate an asymmetry.

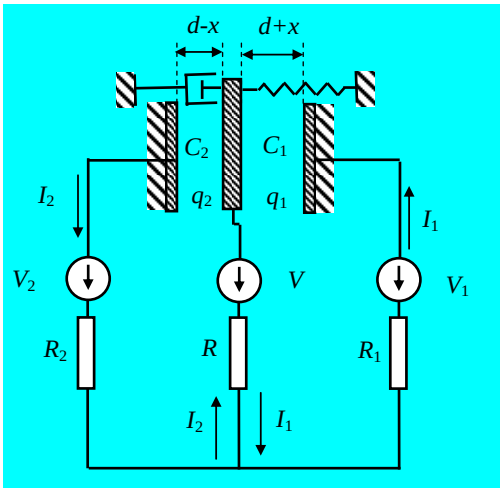

Figure 2: The electro-mechanical diagram sensor with a compensation of an asymmetry

Linearization of Equations and Resonance Operation of the Sensor

The full mechanical and electrical mathematical system describing processes in the sensor were represented by equations (1.20) – (1.22):

Let us consider the next relations in these equations are the next equations:

$$q_1 = q_{1s} + v_1,\ q_2 = q_{2s} + v_2, \tag{1}$$

where q_{1s}=const, q_{2s}=const and parametersv_1 and v_2 depends on time.

The next relation are: $\varphi << \varphi_m$, $v_1 << q_{1s}$, $v_2 << q_{2s}$, and conditions (1.25), i.e. $q_1 = -C_1(V - V_1)$, $q_2 = C_2(V - V_2)$, are valid for q_{1s} and q_{2s} when a rotation angle φ=0. If the compensation condition (1.27) is valid too, it follows from Eqs. (1.4), (1.25) and (1.27) that

$$q_{2s} = -q_{1s} = C_{01}V_3, \tag{2}$$

where V_3 is denoted as $V_3 = V - V_1$.

The system of linear equations may be derived, if Eqs. (1) – (2) and (1.25) are used in Eqs. (1.20) – (1.22) and the linear members with parameters φ, v_1 and v_2 are kept. The steady-state and resonant operations are mostly interesting when measuring periodical signals. The linear system of equations follows to Eq. (34) – (37) after Fourier complex transformation

$$\varphi(\omega) = \frac{M_0\left[1 - \gamma_1 b\omega^2 + j\omega(\tau_1 + \gamma_1\tau_2)\right]}{Z(\omega)}, \tag{3}$$

$$v_1(\omega) = \frac{C_{01}V_3M_0\left[1 - \gamma_1 b\omega^2 + j\omega(\tau + \gamma_1\tau_2)\right]}{\varphi_m Z(\omega)}, \tag{4}$$

$$v_2(\omega) = \frac{C_{01}V_3M_0\left[1 - \gamma_1 b\omega^2 + j\omega(\tau_1 + \gamma_1\tau)\right]}{\varphi_m Z(\omega)}, \tag{5}$$

where

M_0 – amplitude of measured torque,

$$\left.\begin{array}{l}
\tau = RC_{01};\ \tau_1 = (R + R_1)C_{01};\ \tau_2 = (R + R_2)C_{01};\quad p = \tau_1 + \gamma_1\tau_2 \\
b = \tau_1\tau_2 - \tau^2,\ \tau_1 = C_{01}(R_1 + R),\quad \tau_2 = C_{01}(R_2 + R), \\
Z(\omega) = a_0 - a_2\omega^2 + a_4\omega^4 + j\omega(a_1 - a_3\omega^2), \\
a_4 = \gamma_1 I_z b,\quad a_3 = I_z p + \gamma_1 Db,\quad a_2 = I_z + Dp + \gamma_1 I_z b\omega_0^2, \\
a_1 = D + pk - \dfrac{2C_{01}V_3^2}{\varphi_m^2}\left[p + \tau\ 1 + \gamma 1\right],\quad a_0 = k - \dfrac{4C_{01}V_3^2}{\varphi_m^2}.
\end{array}\right\} \tag{6}$$

Also the forth order linear differential equation for parameters φ, v_1, v_2 and their derivatives may be derived at the same time. It follows for parameter v_1 in the form of Eq. (7):

$$a_4\frac{d^4v_1}{dt^4}+a_3\frac{d^3v_1}{dt^3}+a_2\frac{d^2v_1}{dt^2}+a_1\frac{dv_1}{dt}+a_0v_1=q_{1s}\left[M(\omega)+(\omega+\gamma_1\tau_2\frac{dM(\omega)}{dt}\right]. \quad (7)$$

Eq. (38) permits a detailed analysis of transient processes in the sensor.

The linear and nonlinear systems of equations describing the sensor dynamics become singular if $\boldsymbol{\tau}_1$, $\boldsymbol{\tau}_2$ and $\boldsymbol{\tau}$ are vanishing. A problem of numerical computation appears in this case. The order of Eq. (38) has to be lowered then.

It can be seen from Eq. (37) regarding parameter a_0, the additional electrostatic elasticity is brought by electrostatic field and shown in Eq.(39):

$$k_{el}=\frac{4C_{01}V_3^2}{\varphi_m^2}. \quad (8)$$

The parameters τ_1, τ_2 and τ are small. In this case, Eq.(38) is close to an equation of the second order. Then the condition of a resonance in the sensor is derived from an expression for a_0 in Eq. (37):

$$k-k_{el}=I_z\cdot\Omega^2, \quad (9)$$

where Ω is resonant frequency.

This condition has to be imposed on V_3 to secure this resonance. It emerges from Eqs. (8), (9) that

$$V_{3rez}=(-V_{1rez})=\frac{\varphi_m}{2}\sqrt{\frac{1}{C_{01}}(-I_z\Omega^2)}. \quad (10)$$

The member $\gamma_1 b\omega^2 << 1$ and this member can be neglected, because the parameters τ_1, τ_2 and τ are small. Therefore if Eqs. (8) and (9) are used, the member $Z(\omega)$ in formulas (6), can be rewritten as

$$Z(\omega)=I_z(\omega^2-\Omega^2)+D\omega^2(1+\gamma_1\tau_2)-j\omega D_{eq}, \quad (11)$$

where the equivalent damping coefficient is

$$D_{eq}=D+\frac{1}{2}(-I_z\Omega^2)C_{01}(R_1+\gamma_1R_2). \quad (12)$$

The frequency response for currents $I_1(\omega)$ and $I_2(\omega)$ can be derived from Eqs. (1), (4), (5) as $I_1=j\omega v_1$, $I_2=j\omega v_2$, because $I=\frac{dq}{dt}$ It follows with high accuracy from Eqs. (4), (5) that $I_2\approx I_1$ with inaccuracy up to $\omega\tau$.

Figure 1 shows that currents I_1 and I_2 have opposite directions in a resistor R. These currents have to be subtracted at the output to form a maximum output current of the sensor. Then, the frequency response of the output current is taken from $I_1=j\omega v_1$ and Eqs.(4), (11) and (12), if the middle member in the right side of Eq.(11) is neglected:

$$I_{out}(\omega) = 2I_1(\omega) = \frac{M_0\omega\sqrt{C_{01}(-I_z\Omega^2)}}{\sqrt{I_z^2(\omega^2-\Omega^2)^2+\omega^2 D_{eq}^2}}. \quad (13)$$

The resonant value of I_{out} may be determined from Eq. (13), if $\omega=\Omega$:

$$I_{rez} = 2I_{1rez} \approx \frac{M_0\sqrt{C_{01}(-I_z\Omega^2)}}{D_{eq}}. \quad (14)$$

The sensor's sensitivity to input torque is defined as ratio $K_M = \frac{I_{out}}{M_0} = \frac{2I_1}{M_0}$. Then this sensitivity follows from Eq.(13) as

$$K_M(\omega) = \frac{\omega\sqrt{C_{01}(-I_z\Omega^2)}}{\sqrt{I_z^2(\omega^2-\Omega^2)^2+\omega^2 D_{eq}^2}}. \quad (15)$$

When $\varphi=\Omega$ from Eq.(3), and the same as above the resonant value of angle φ becomes:

$$\varphi = \varphi_{rez} \approx \frac{M_0}{D_{eq}\Omega}. \quad (16)$$

The maximum torque may be measured at a resonant operation determined from the condition $\varphi_{rez} \le \varphi_s$ and from Eqs. (1.30), (10) and (14):

$$M_{0\max} = \varphi_m D_{eq}\Omega\sqrt{1-\sqrt{1-\left(\frac{\Omega}{\omega_0}\right)^2}}. \quad (17)$$

The dynamic working interval of the sensor may be defined by Eq. (18).

$$D_w = \frac{M_{0\max}}{M_{0\min}}. \quad (18)$$

The transient current process in the sensor follows to the formula (19), if energy dissipation is not too big, because here the exponential decay rate is $\delta_{eq} = D_{eq}/(I_z)$:

$$I(t) \approx I_{out}\left[1-\exp\left(-\frac{1}{2}\frac{D_{eq}}{I_z}t\right)\right]\cos(\omega t). \quad (19)$$

It has to be noted that $\delta_{eq} > 0$ whereas it can be positive or negative in the resonant capacitive sensors which external or inner generators are in electrical excitation circuits (see formulas (1.1)).

The current I_1 can be determined from what was above as

$$I_1(t) = -q_{1s}\frac{1}{\varphi_m}\frac{d\varphi(t)}{dt}. \quad (20)$$

It means that the sensor realizes a direct transformation of an angular velocity of SP into a current, while the most of known capacitive sensors realize a direct transformation of a moving plate displacement into a charge or a voltage.

The Effect of Energy Dissipation In Elastic Torsion Bar

There are two types of mechanical energy dissipations in the sensor: the external dissipation, in which energy is lost into the environment, and internal dissipation, where energy is ultimately lost as heat within the system [2]. The first type dissipation is the existing friction torque $M_{ext\,fr} = D_{eq}\dot{\varphi}$ or $M_{ext\,fr} = j\omega D_{eq}\varphi$, if SP rotations are harmonic. In this case, if W is the total energy stored in any macroscopic oscillator and ΔW is the energy dissipated with one cycle of oscillation with frequency ω, then the dimensionless quality factor Q of the oscillator is

$$Q_{ext}^{-1} = \frac{1}{2\pi}\frac{\Delta W}{W} = \frac{D_{eq}\omega}{I_z\omega_0^2} = \frac{D_{eq}\omega}{k}. \tag{21}$$

The D_{eq} is supposed to be a constant in linear systems. It follows from Eq. (21) that the energy dissipation and external friction are frequency dependent (FD).

The second type of mechanical energy dissipation is an internal friction in materials. This dissipation arises from a process called 'anelasticity' [2]. For an inelastic material the strain response lags behind the applied stress, developing over a finite relaxation time. In the harmonic processes this appears as a phase lag 'ϕ' between the applied force and the response of the system, known as the loss angle. In this case the energy dissipation may be described with friction torque $M_{\text{int}\,fr} = jk\varphi$ [2].

It can be shown that the loss angle is a measure of the fractional energy dissipated per cycle of oscillation [2, 3]. Thus the energy losses are caused by an internal friction described with the following relationship

$$\frac{1}{2\pi}\frac{\Delta W}{W} = Q_{\text{int}}^{-1} = \phi. \tag{22}$$

Many authors have reported that the internal friction in a wide variety of materials is largely frequency independent (FI) [2]. However, materials may have several so called Debye's peaks at frequencies separated by many orders of magnitude. All metals have inherently the same order losses (10^{-3} – 10^{-4}) at frequencies on the order of one to a few tens of Hz [3]. Two examples dependences $\phi(f)$ in this frequency interval are shown in Fig. 2. The dots are experimental data and the solid curves are approximation using Zener model which follows the model in [3].

$$\phi(f) = \phi_0 + \Delta\frac{f / f_r}{1 + (f / f_r)^2}, \tag{23}$$

where ϕ_0, Δ and f_r are fitted values are reported in Table 1.

Table 1: Internal friction fitted parameters for two samples

Material	$\phi_0\ 10^4$	$\Delta\cdot 10^3$	f_r, (Hz)
C85 Steel	1.9 ±0.1	1.9 ± 0.4·	480 ± 20
Chrome Alloy	0.9 ± 0.5·	2.0 ± 0.1	135 ± 8

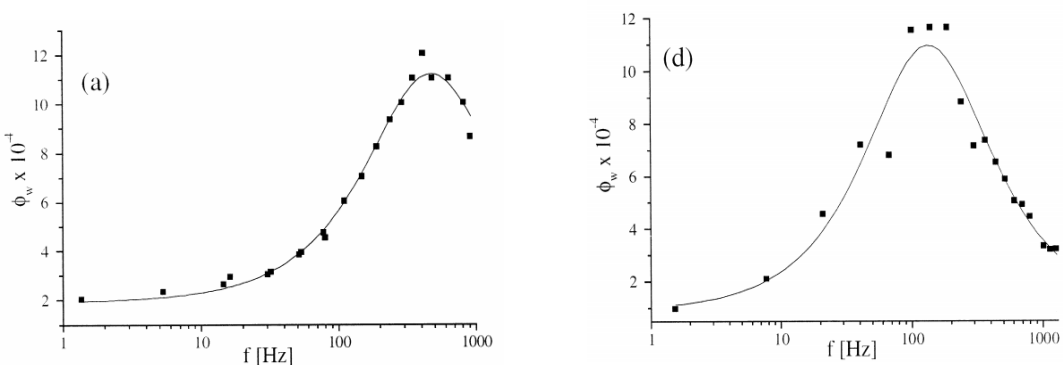

Figure 2 [3]: The internal friction ϕ versus frequency ω in thin wires of (a) C85 steel and (d) Chrome Alloy at room temperature T = 300 K. The wires diameter is 0.25 mm.

The sensor under design is supposed to work near frequency of one Hertz. It follows from Table 1, Eq. 23 and Fig. 9 that near this frequency

$$\phi(f) \approx \phi_0 = const. \tag{24}$$

Here $\phi_0 \approx 2\cdot 10^{-4}$ is used for the sensor under design following Table 1.

In common case the friction torque, when both types of energy dissipation are acting is

$$M_{fr} = M_{ext\,fr} + M_{\mathrm{int}\,fr}\,. \tag{25}$$

Thus the theoretical results above can be used to design the sensor if the parameter D_{eq} (Eq. (12)) is substituted with the parameter:

$$D_{com} = D_{eq} + \frac{\phi_0 k}{\omega} = D + \frac{\phi_0 k}{\omega} + \frac{1}{2}\left(-I_z\Omega^2\right)C_{01}\left(R_1 + \gamma_1 R_2\right). \tag{26}$$

Also, the common quality factor can be defined similar to formula (52):

$$Q_{com}^{-1} = \phi_0 + \frac{D_{eq}\omega}{k} = \phi_0 + \frac{\omega}{k}\left[D + \frac{1}{2}\left(-I_z\Omega^2\right)C_{01}\left(R_1 + \gamma_1 R_2\right)\right]. \tag{27}$$

Dissipating ratio ζ and exponential dissipation coefficient δ_{com} follows the well known formulas in [4-6]:

$$\zeta = \frac{D_{com}}{2\sqrt{kI_z}} = \frac{D_{com}}{2I_z\omega_0}, \qquad \delta_{com} = \zeta\omega_0 = \frac{D_{com}}{2I_z}\,. \tag{28}$$

The Thermal Noise of the Sensor

The sensitivity of any measuring instrument is limited by the background thermal noise. It is worth noticing that a calculation of this noise in case of nonlinear physical system is valid only if a linearization of dynamic equations of this system is carried out [7]. That is why the linear equations that have been derived previously will enable to estimate this noise level.

A thermal noise is caused by processes of energy dissipation in the sensor [2, 8, 9]. The effect of this noise on SP is considered as an imaginary external fluctuating torque. The power spectral density (PSD) of this torque follows to well-known Eq.(29) found also in [2, 3, 8, 9].

$$S(f) = 4k_B T D_{com}, \tag{29}$$

where k_B – is the Boltzmann constant, T is the absolute temperature.

The PSD of the sensor's output thermal noise current can be received from Eqs. (15) [10]:

$$S_{th}(\omega) = 4k_B T D_{com} K_M^2 = \frac{4k_B T C_{01}^2 (-I_z \Omega^2) D_{com} \omega^2}{I_z^2 (\omega^2 - \Omega^2)^2 + \omega^2 D_{com}^2}. \tag{30}$$

It is supposed here that the sensor's output harmonic signal with Ω frequency has been measured during a time t_m. Thus this generates a natural time window with a rectangular view function. A production harmonic signal and a rectangular view function form a spectral window in frequency region [11, 12], which for random signals follows Eq.(62) [11].

$$S_W(\omega) = \frac{t_m}{2}\left[\frac{\sin(\omega - \Omega)\frac{t_m}{2}}{(\omega - \Omega)\frac{t_m}{2}}\right]^2. \tag{31}$$

The function $S_W(\omega)$ is exposed in Fig. 3:

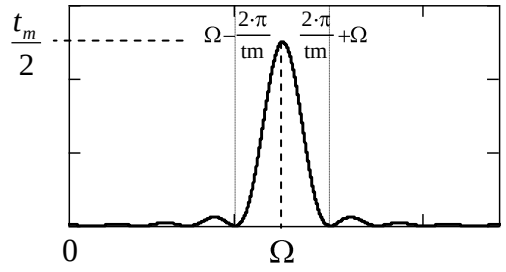

Figure 3: The spectrum window due to a finite measuring time t_m.

Fig.3 shows that the spectral window is transparent for frequencies ω that are mostly within interval $\Omega - \frac{2\pi}{tm} < \omega < \Omega + \frac{2\pi}{tm}$. The root mean square of the fluctuating thermal noise current issues from Eqs. (30), (31) and follows to formula (32)

$$I_{th} = \sqrt{\frac{1}{2\pi}\int_{\Omega-\frac{2\pi}{t_m}}^{\Omega+\frac{2\pi}{t_m}} S_W \left(S_{th} \right) dx} \,. \qquad (32)$$

Design and Construction of the Differential Capacitance Instrument

The sensor is designed as a monoblock device with Titanium Alloy (E= 114 MPa, G=41 GPa and density 4.6 Mg/m^3) suitable for the casing having sufficient stiffness for the torsion pins to reduce fatigue and conserve elasticity with a sensor subject to frequent torsions.

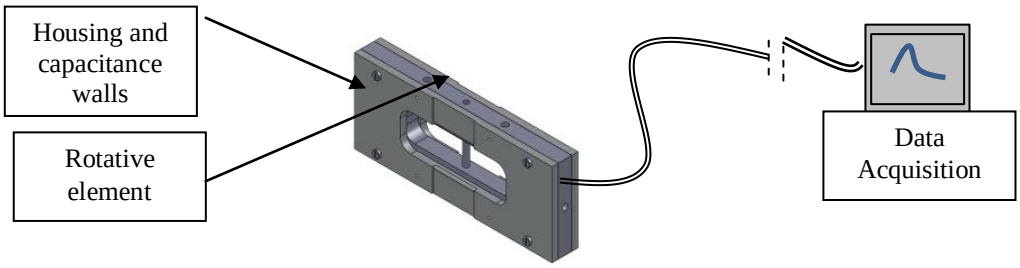

Figure 4: Differential capacitance instrument.

The modulus of elasticity is within a range to produce a torsional stiffness of the pins such that the rotation resonant frequency is within the application desired range. The instrument is designed as shown in figure 4. Its natural frequency is 10 Hz when an electrostatic field is switch out. The more voltage of a main source in this device the more it is sensitive. A maximum voltage in a vacuum is limited with 500 V. For the sake of reliability we can be limited with 400 V.

Numerical Calculation of The Sensor's Parameters

It is interesting to calculate the design parameters and the magnitude of an output signal in the sensor when a smallest gravitation torque $M_{0\min}$ acts as an input signal. Such torque can acts in inhomogeneous gravity field. As it was mentioned in Part 1, in gravity gradiometer the torque is $M_0 \approx I_z \Gamma$. Usually the minimum value of a $\Gamma_{\min}$ is considered as 10^{-9} s^{-2} [13-18]. For a better understanding of this value, an analogous sensor can be considered which measures a linear acceleration *a*. In this case the SP has to have a static imbalance *s* [19]. Let the torque due to this imbalance be $M_0\ a\ = m.a.s = 1.0 \cdot a \cdot \text{gram cm} \approx 10^{-4} \frac{a}{g}$ Nm.

Let $I_z=5\cdot10^{-4}$ kg·m^2, then $M_{0\min} = I_z \Gamma_{\min} = 5\cdot10^{-13}\,\mathrm{N}\cdot\mathrm{m}$, it can be seen that the correspondent linear accelerometer is measuring an acceleration $a\approx5\cdot10^{-9}$g.

As an example, the specified parameters of the sensor are reported in the table 2 (all parameters are in SI units).

Table 2: The specified sensor's parameters

$d=1\cdot10^{-4}$	$\gamma=0.1$	$k=2$	$R_1=R_2=R=20$
$r=0.05$	$t_m=10$	$I_z=5\cdot10^{-4}$	$M_{0\ \min}=5\cdot10^{-13}$
$s=1.6\cdot10^{-3}$	$\Omega=2\cdot\pi$	$\omega_0=2\cdot\pi\cdot10.07$	

The differences between both effects on the sensor dynamics of the external and internal frictions will be found out. The cases where $D_1=0$, $\phi_{01}=2\cdot10^{-4}$ (FI type energy dissipation) and $D_2=6.366\cdot10^{-5}$, $\phi_{02}=0$ (FD type energy dissipation) will be analyzed. The value D_2 is considered to have the following equality

$$D_2 = \frac{\phi_{01} k}{\Omega}. \tag{33}$$

This gives energy dissipations equality at resonance frequency for both types of energy dissipations.

The dependences I_{out} on a stiffness k for both effects are determined from Eqs. (12), (26) and are represented in Fig. 5. This figure is complemented with Fig. 6 where the dependence V_{3rez} on k is shown.

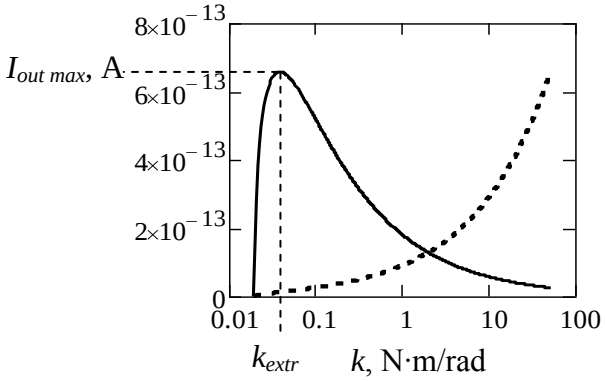

Figure 5: The dependence I_{out} on k. Solid curve corresponds to FI type energy dissipation (inner friction), dashed curve corresponds to FD type energy dissipation (external friction).

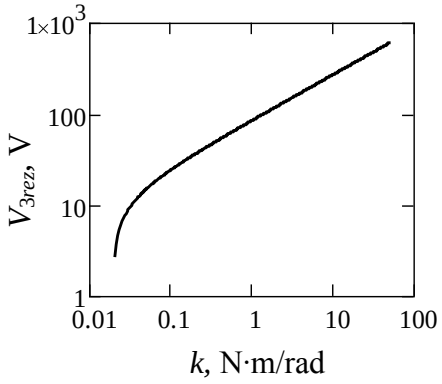

Figure 6: The dependence V_{3rez} on k (from Eq. (10))

The current's maximum existence deserves to be noted in Fig. 5. The parameters of this maximum are:

$$I_{out\max} = \frac{M_0}{2\phi_0}\sqrt{\frac{C_0}{I_z}}, \quad k_{extr} = 2I_z\omega^2. \tag{34}$$

The resonant curves for current I_{out} and transient process for both dissipation types are shown in Fig. 7.

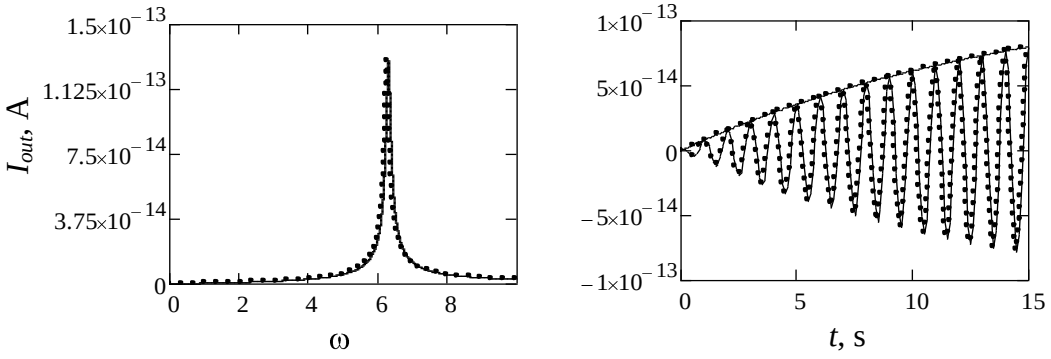

Figure 7: The sensor frequency responses and transient processes for both energy dissipation FI type (Solid curves) and FD types (dotted curves) if it is an equality (33)

It can be seen from Fig. 7 that the resonant and transient processes coincide for both types of energy dissipations if equality in Eq.(32) is held.

Fig.8a) shows the noise reduction with increasing parameters ϕ and D. It can be explained with distortion sensor's amplitude-frequency characteristic while the measurement frequency interval is a constant (See Fig.3) but full fluctuation energy doesn't depend on D_{com} (the D and D_{com} are in SI unit). On the other side, Fig.8 b) demonstrates the absence of thermal noises limitations in the sensor with chosen specific parameters reported in Table 2, because $I_{out} / I_{th} > 1$.

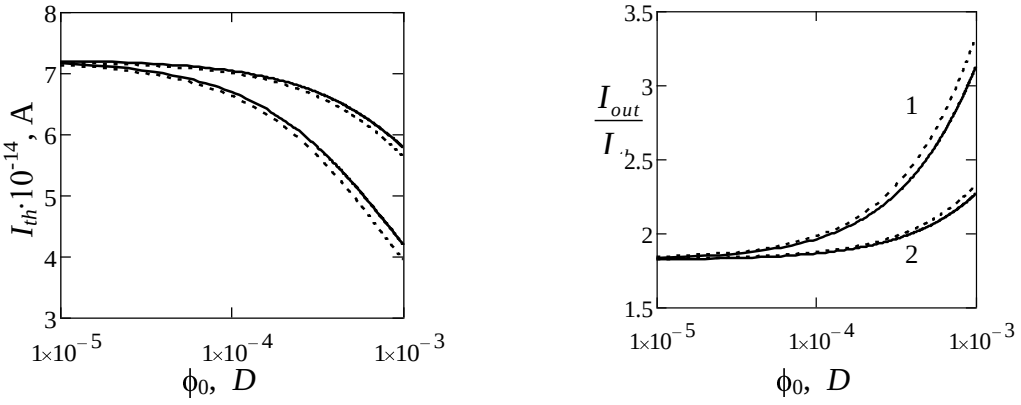

(a) **(b)**

Figure 8: a) Dependence output current RMS on parameters ϕ_0 and D at two different values of t_m. b) Dependence ratio signal/noise on parameters ϕ_0 and D at two different values of t_m

All data are received at resonant frequency when $I_{out}=1.3\cdot10^{-13}$ A. Solid curves are for $t_m=1$ s; dashed curves are for $t_m=10$ s. Curves 1 are dependent on D ($\phi_0=2\cdot10^{-4}$); curves 2 are dependent on ϕ_0 ($D=D_2=6.366\cdot10^{-5}$ N·m/(rad/s)).

A set of derived design parameters for the gravity gradiometer sensor are reported in Table 3 (all parameters are in SI units). Here it is assumed that the sensors movable details are in vacuum so that an inner friction in elastic torsion bar and electrical resistance are mechanisms of energy dissipation.

Table 3: The derived sensor's parameters if $D=0$, $\phi_0=2\cdot10^{-4}$

$V_{3rez}=118.593$ $\varphi_s=1.4\cdot10^{-4}$ $\varphi_{rez}=1.25\cdot10^{-9}$ $\varphi_m=2\cdot10^{-3}$	$D_{com}=6.4\cdot10^{-5}$ $M_{0\ max}=9.0\cdot10^{-9}$ $D_W=1.2\cdot10^{5}$ $C_{01}=1.408\cdot10^{-10}$	$\zeta=0.001$ $\delta=0.064$ $Q_{com}=5\cdot10^{3}$	$I_{out}=1.3\cdot10^{-13}$ $I_{th}=4.5\cdot10^{-14}$ $I_{out\ max}=6.6\cdot10^{-13}$ $k_{extr}=0.039$

Comment 1. One needs to take D_{com} instead of D_{eq} to estimate the sensor's parameters that are related to energy dissipation with equations discussed earlier. Also one needs to take a resonant frequency Ω instead of frequency ω in Eq. (26) – (27).

Comment 2. The conditions (1.27) and (10) contain a one free parameter. It may be one of the voltages V, V_1 or V_2. In principle it enables to make choosing voltage's values more comfortable. For example, if $V=60$ Volt from conditions (1.27) issues V_1=-58.593 Volt; V_2=-47.812 Volt. There are other variants dividing the voltage 118.593 Volt between these three voltage sources.

An Example of an Output Circuit of The Sensor

The electric output sketch of the sensor is shown in Fig. 9. The OP-amplifiers with resistors R_3 are current-to-voltage convertors. The voltages $\pm V_4$ are I_2R_3 and $-I_1R_3$, if the OP-amplifiers are assumed to be ideal. These both voltages are subtracted in a differential OP-amplifier with resistors R_5. The output voltage is $V_{out} = 2I_1 \cdot R_3 \cdot \frac{R_5}{R_4}$ [20]. If I_{out}=10^{-13} A; R_3=10^7 Ohm and ratio R_5/R_4=10^4, the output voltage is $V_{out} \approx 0.01$ Volt . This value allows the implementation of a signal sequential processing.

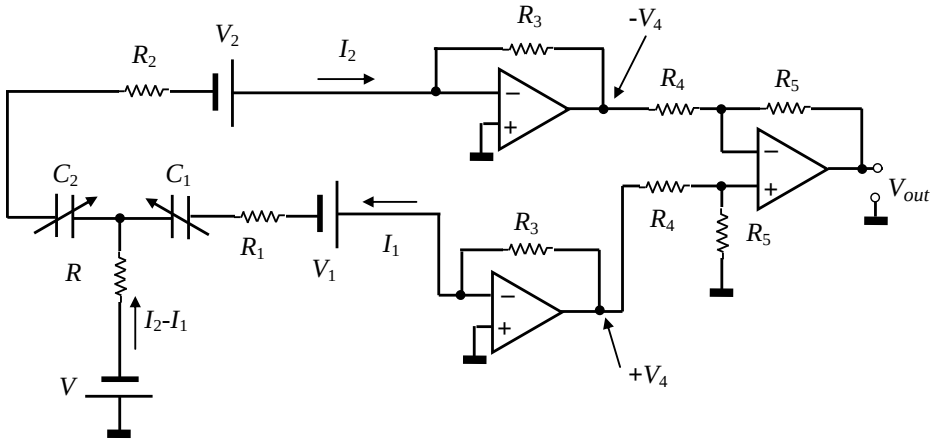

Figure 9: The sensor's output electric sketch

Conclusion

This sensor is intended to measure harmonic signals, such as linear and angular accelerations and second derivatives of gravity potentials. The sensor's construction combines a dual function of an electrostatic capacitive differential sensor and electrostatic capacitive actuator without any additional generators or alternative electric voltage sources for a power supply. The actuator permits to decrease the resonance frequency of the sensor and by-turn this actuator permits to use a harder elastic hanger for sensing plate (SP). Also the actuator permits a resonant frequency tuning.

The sensor is very simple but needs attention in the design and assembly. It needs a constant voltage as an energy supply source and three plates for fabrication, one of them (SP) can rotate in an elastic hanger. This sensor realizes a direct transformation of an angular velocity of SP into an output current, while the most of known capacitive sensors realize direct transformations of a SP displacement into a charge or a voltage.

The electrical asymmetry in differential capacitors imposes severe restrictions on the sensor fabrication as it was shown in Part 1. There it was shown also the additional voltage source is able to compensate this asymmetry.

The nonlinear dynamic equations describe the dynamic and signal transformations of the sensor. The conditions of static and dynamic stabilities of the SP have been investigated in Part 1. These equations were transformed into a linear one in Part 2. Here the various regimes of operation of the sensor including transient state, regimes of harmonic oscillations and a resonant one were considered.

The input signals in the sensor are torques of noncontact inertial and gravitational forces which act on a SP. The output signal is a sum of currents I_1 and I_2 of two capacitors. Currents frequency is equal to a frequency of an input signal.

The design parameters for the sensor (see Table 3) is indented to measure the second derivation of gravity potential with magnitude $\Gamma=10^{-9}$ s^{-2} were calculated in Part 2. The constant voltage source allows a having a resonant frequency of one Hertz, while the natural frequency of the SP in an elastic hanger is about 10 Hertz, if a resonant voltage is 118.593 Volt. The amplitude of output current is $I_{out}\approx 1.3\cdot 10^{-13}$ A in this case. Here it was shown this small current can be transform into a voltage about 0.01 Volt by the modern current-to-voltage convertors and OP-amplifiers in the sensor's output electric circuit.

Two type energy dissipations were considered: one is dependent on a frequency and other is independent on one. It is shown the maximum of sensor's sensitivity versus on hanger's elasticity exists in last case.

The estimations of thermal noise and of signal - to - noise ratio in the sensor were given. The designed theory can be used for electrostatic sensors with elastically attached bodies.

Acknowledgment

The authors would like to thank King Fahd University of Petroleum and Minerals, DSR Research Office and Belarusian National Technical University for their support of this research.

References

[1] I.Gilavdary, S.Mekid and N. Riznookaya, Differential-Capacitance Instrument for Measurements of Inertial and Gravitational Forces and Torques: Theory and Analytical Design (Part 1). International Journal of Applied Engineering Research, Volume 9, Number 23 (2014) pp. 23119-23132.

[2] I. W. Martin. Studies of materials for use in future interferometric gravitational wave detector. Presented as a thesis for the degree of Ph.D. The University of Glasgow, 2009. P. 225. (https://gwic.ligo.org/thesisprize/2009/Martin_Thesis.pdf)

[3] G. Cagnoli, L. Gammaitoni, J. Kovalik, F. Marchesoni, M. Punturo. Low-frequency internal friction in clamped-free thin wires. Physics Letters (A 255), 1999, pp. 230-235. (http://www.nipslab.org/files/sdarticle_4.pdf)

[4] http://en.wikipedia.org/wiki/Damping_ratio.

[5] S. G. Kelly. Theory and problems of mechanical vibrations. New York, 1996.
[6] Vibration and Shock Handbook. Edited by Clarence W. de Silva. Taylor and Francis Group. 2005.1771 P. (http://libgen.info/view.php?id=130227)
[7] W. Bernard, H.B. Callen. Irreversible Thermodynamics of Nonlinear RC-System. Phys. Rev. 118, No 6, 1466, 1960.
[8] H. B. Callen. T. A. Welton. Irreversibility and generalized noise. Physical Review 83 (1951) 34-40.
[9] R. F. Greene. H. B. Callen. On the formalism of thermodynamic fluctuation theory, Physical Review 83 (1951) 1231-1235.
[10] J.S. Bendat, A.G. Piersol. Engineering Applications of correlation and spectral analysis. A Willey-Interscience Publication, 1980.
[11] J.Max. Methodes et techniques de traitement du signal et applications aux mesures physiques. Tome I. Principes generaus et methodes classiques. 1981.
[12] G.R. Cooper and C.D. McGillem, Probabilistic Methods of Signal and System Analysis, New York, Oxford University Press. 1986.
[13] R.L. Forward. Measurement of static field gradient. US Patent No 3273397. Filed 05.06.1964.
[14] C.C. Bell. Torsionally resonant gravity gradient sensor. US Patent No 3564921. Filed 23.02.1971.
[15] M.U. Sagitov, V.S. Nazarenko, B. Bodri, Kh.G. Tadzhidinov. Lunar Gravimetry. Academic Press, Harcourt Brace Jovanovich, Publishers. London, Orlando, San Diego, New York, Austin Boston, Sydney, Tokyo, Toronto. 1986, 309 P. (http://libgen.info/view.php?id=253990)
[16] W. Torge. Gravimetry. Water de Gruyter. Berlin-New York, 1989, 465 P.
[17] Jekeli C. The gravity gradiometer survey system GGSS). // EOS. Trans. Amer. Geophys, 1988, v. 69, No 8. – pp. 105, 116–117.
[18] D. DiFrancesco, A. Grierson, D. Kaputa and T. Meyer. Gravity gradiometer systems – advances and challenges. Geophysical Prospecting, 2009, 57, pp. 615–623.
[19] Y. Lin, M. Fuhrmann, A.C. McNeil. Symmetrical differential capacitive sensor and method of making same. United States Patent Application Publication. Pub. No. US 2009/0031809 A1.
[20] W. Kester. Practical Design Techniques for Sensor Signal Conditioning. Analog Devices, 1999, 366 P. (http://www.scribd.com/doc/7274187/ Practical-Design-Techniques-for-Sensor-Signal-Conditioning. Analog-Devices).